International Journal of Applied Engineering Research ISSN 0973-4562 Volume 12, Number 13 (2017) pp. 3978-3987

Simulation of Auxetic Behavior in Planar Random Steel Fiber Networks

Mehmet Seha Tatlier

Assistant Professor, Department of Mechanical Engineering, Osmaniye Korkut Ata University, Osmaniye, Turkey.

Umut Aksu

PhD Student, Department of Mechanical Engineering, Osmaniye Korkut Ata University, Osmaniye, Turkey.

Abstract

The materials possess negative Poisson's ratios are called auxetic materials. Although it is rarely available in the nature, they naturally occur in various organic and inorganic materials. Auxetic materials have distinct and advantageous behavior that can be exploited in different applications. Most of auxetic materials have porous structures, which make them vulnerable for structural applications. One of the best ways to overcome such a short come is to develop composites both are strong enough for structural application and auxetic for benefiting from the negative Poisson's ratios for specific applications. It is known in literature some random fiber network of stainless steel fibers exhibit auxetic behavior. These networks can be employed in a stronger matrix in order to develop structurally robust auxetic composites. However, before such an approach can be developed, a methodology for designing fibrous networks with the desired negative Poisson's ratios must first be established. This requires a deep knowledge about the parameters affecting the auxetic behavior in these kinds of networks. In this work, we present a modelling approach to study the auxetic behavior of compressed fused fibrous networks. Finite element analyses of three-dimensional stochastic fiber networks were performed to gain insight into the effects of parameters such as network anisotropy, fiber morphology and degree of network compression on Poisson's ratio. In this study, the network compression ratio and anisotropy are found to be two key parameters playing important roles in the tailoring the auxetic behavior at fiber networks of stainless steel. In addition, one other outcome of this study is that 2D fiber network model responses in an analogous manner with 3D fiber network model. Hence, the 2D fiber network model can be employed for investigation of auxetic behavior fibrous networks instead of 3D models yielding less numerical cost.

Keywords: Anisotropy, Auxetic, Compression, Effective Young's Modulus, Poisson's ratio

INTRODUCTION

A competitive world obliges the continuous development in engineering and technology, which is accompanied by material advancements. Composites are among the most favored materials utilized in new high-performance applications. Advances in composite materials are greatly appreciated by the aerospace industry where they possibly reduce the weight of new generation airplanes by almost 50% in new generation allowing further flight with less fuel and emission in absence of compromising any strength and stiffness values [1].

Tests performed by Delannay [2, 3] on some sintered metal fiber mats and fibrous papers have shown negative Poisson's ratios. However, research toward the design and development of auxetic random fibrous networks is inadequate compared to the other fields of auxetic materials research. This study is centered around the development of a numerical model that helps to determine parameters affecting the mechanical properties and deformation mechanisms of auxetic random fibrous networks. Ultimately, properties enhanced by numerical model can lead to a new generation of auxetic composites utilizing random fibrous networks as reinforcements.

Insight of the current state of knowledge is the first and essential step for all research incentives as well as for this study on the design and development of auxetic random fibrous networks. As mentioned previously, most of the auxetic materials known today are either manmade or found both in organic and inorganic materials naturally. Thus, a review of previous studies on auxetic materials is presented below.

NATURAL MOLECULAR AUXETIC MATERIALS

A negative Poisson's ratio was first discovered in iron pyrites [4]. The scientists accepted it cautiously although the elasticity theory permitted such phenomenon. Single crystal materials such as arsenic [5] and cadmium [6] were discovered to show negative Poisson's ratio. In addition Baughman et al. [7] has determined that the majority of the cubic elemental metals and

some rare gas solids with a FCC structure exhibit auxetic behavior if they are subjected to a specific stretching direction.

Later, naturally occurring silicate α-cristobalite with a negative Poisson's ratio in a specific loading direction was independently discovered and reported by Kasker and Chelikowsky [8] using ab initio modeling technique and by Yeganeh-Haeri et al. [9] who experimentally measured the mechanical properties of silicate α-cristobalite. The experiments done by Yeganeh-Haeri show that a negative Poisson's ratio occurs in (100) and (010) planes under the loads which lie in those planes. The deformation mechanism of the α-cristobalite silicate was first explained by the rotation of rigid SiO_4 tetrahedras by Kasker and Chelikowsky [8]. Alderson et al. [10, 11, 12] explained the auxetic behavior with a concurrent tetrahedral model. Recently, Grima et al. [13] proposed a rotating rectangles model, after observing molecular structure of the atoms in the deformation planes. The auxetic behavior in silicate α-cristobalite was explained by Grima et al. [14] with the synchronous rotation and translation of rotating rectangles representing the projections of the atomic positions of silicate α-cristobalite on (100) and (010) planes.

Some living organisms have also adapted the negative Poisson's ratio at certain parts of their bodies to exploit the benefits of auxetic properties. The literature is still limited in auxetic biomaterials because the determination of the mechanical properties of living organisms in their natural environment is challenging. However, cow teat [15], cat [16], and salamander skins [17] were identified to have negative Poisson's ratios. The negative Poisson's ratio is believed to be the cause of complex microstructural fibers in these skins. Some load-bearing cancellous bones from human shins have also been reported to exhibit auxetic behavior [18] due to their specific cellular structures. Biomedical engineers must also take auxetic functionality into account to accomplish sufficient match between biomaterials and synthetic replacements during the design and development of synthetic replacement products.

MANMADE AUXETIC MATERIALS

New materials with enhanced mechanical properties are highly demanded by developing technology. One of the accepted approaches in tailoring various material properties is the manipulation of Poisson's ratio. For example, shear modulus G and bulk modulus K depend on Poisson's ratio and Young's modulus as seen in Eq. (1). In a structural application, shear modulus is desired to be larger than its bulk modulus [19]. Because high shear modulus allows a material to sustain larger shear loads while low bulk modulus induces less resistance to volume change. In other words, Poisson's ratio must be modified if the ratio of shear modulus to bulk modulus is required to be greater than 1.0. The ratio of shear modulus to bulk modulus grows infinitely large as Poisson's ratio approaches -1.0 in Eq.(1).

$$\frac{G}{K} = \frac{3(1-2\nu)}{2(1+\nu)} \geq 1 \qquad (1)$$

One of the earliest adoptions of auxetic effects in a practical application was in a magnox nuclear reactor moderator by which free neutrons are slowed down. The horizontal plane of a magnox moderator is composed of radially keyed graphite. Freestanding graphite bricks are radially connected to each other and the entire structure can be approximated to an anisotropic continuum material [20].

The basic idea of keyed brick construction is to obtain the largest resistance against shear forces that can be executed by an earthquake while allowing free movement of the structure to accommodate differential deformation between the graphite bricks and the steel supporting structures at the edges of the core. The shear modulus grows infinitely large with respect to bulk modulus when Poisson's ratio is -1 as also mentioned in Eq.(1).

The 2D re-entrant honeycomb cellular solids were among the first developed auxetic materials. They consist of macroscopic cells with various dimensions. The deformation mechanism is due to hinging and flexure of diagonal ribs under tensile loads. Auxetic cellular structures have a significant potential in nanotechnology and MEMS as well as for core materials of sandwiched composites. In addition, re-entrant honeycombs are mainly used in filtration applications although their manufacture is hard and costly. Auxetic honeycomb structures can be used in smart filtration systems where particulate selectivity is achieved with auxetic behavior. However, in order to utilize auxetic honeycombs in full capacity, cell sizes in re-entrant honeycombs are required for further scale-down. The dimensions of cellular auxetic materials are brought down to 10μm- 1μm by laser lithography [21]. The silicon surface micromachining technique is utilized to obtain dimensions around a tenth of 1 μm [22]. Furthermore, with nanofabrication techniques, dimensions around 100 nm can be achieved.

The development of auxetic polyurethane (PU) by Lakes [20] was an important discovery in auxetic research. Poisson's ratios for polymeric and copper foams are reported to be $\nu = -0.7$ [20] and ν=-0.8 [23], respectively. Transformation from conventional to auxetic foam is achieved with an innovative technique developed by Lakes [20]. PU foam is compressed triaxially above softening temperature and cooled down to room temperature under compressive loads during which solidifying of cell structures into permanent re-entrant cell geometries occurs. The different cell structures are well distinguished from the pictures taken with scanning electron microscope (SEM). A negative Poisson's ratio [24] results from these re-entrant cell structures whose deformation characteristics are explained by Grima et al. [25] with his rotating triangles model. Re-entrant cell structures transform from convolute to convex geometry when they are subjected to

tensile loadings. The deformation mechanism is explained with the rotating triangles analogy.

Caddock and Evans have found an expanded form of polytetrafluoroethylene (PTFE) that shows a negative Poisson's ratio [26]. In addition to a Poisson's ratio as low as $\nu = -12$, PTFE attains a higher strength than PU foams.

Modeling and morphological studies on PTFE revealed that the auxetic behavior was associated with the microporous structure rather than its intrinsic properties. The microstructure of PTFE consists of nodules and fibrils. This re-entrant like structure, where nodules are interconnected with fibrils is responsible for negative Poisson's ratio behavior. Auxetic PTFE that is used in dilators for coronary angioplasty had a substantial advantage over non-auxetic PU dilators. The benefits of auxetic PTFE dilators come from the extraction of dilators during the forward movement and contraction during the pull.

Industries that are using numerous non-auxetic composites in their current designs with high strength- and stiffness-to-weight ratios will also benefit from the advantages of auxetic behavior with the development of auxetic composites. Sequential piling of angle-ply reinforced laminates and composites with one or more auxetic composites are two well-known techniques in the development of auxetic composites.

MODELING

The modeling discussed in this section includes an in-plane 2D network model. The numerical investigation of the fiber networks can be divided into two main parts: generation of the geometry and finite element analysis of the model. The first part mentioned above accepts manual data for specific requirements of the network and creation of the fiber networks. The generation of fiber networks are performed by MATLAB, which is a higher-level compiler with many available built-in functions. MATLAB has significant advantages in array and matrix operations as compared to other high-level compilers. The second part discussed is the numerical static analysis of generated fiber networks. The commercially available software Strand7 is utilized where fibers are modeled as beam elements with rigid connections.

NETWORK GENERATION

Random fibrous networks have complicated geometrical structures. An adequate representation of this intricate geometry is developed effectively with computer code created in MATLAB. Initially this code generates center points by assigning random ordinates depending on the simulation cell dimensions of the networks. Simultaneously, for each center an in-plane angle θ is also randomly input for 2D networks.

PERCOLATION

A percolating cluster is the connected network of fibers bridging to opposite sides of the simulation volume. In order to perform numerical analysis, a percolating cluster must be established. After periodic boundary conditions is established, percolation routine in the code determines the percolating cluster. Fibers that are not connected to the percolating cluster are removed to have positive definite stiffness matrix in the solution procedure. The non-load-bearing parts of fibers are removed for less computational use and for more clear geometries.

FINITE ELEMENT MODEL FOR FIBERS

In this study, effective E and ν of random fiber networks are investigated. In order to obtain the overall properties of fiber networks, microstructural modeling of fibers is required. Deflection of a fiber is given by the solution of a partial differential equation. Although deflection of a fiber can be analytically solved, for intricate models an approximate solution is needed.

The finite element method is used to obtain the effective Young's modulus and Poisson's ratio properties of the network. This is achieved by dividing the fibers into the beam and the contacts into the rigid elements. Even though finite element solution is not as complicated as analytical solutions, models should be constructed carefully in order to closely interpret the real situation. Predefined material properties in Strand7 for Stainless Steel Grade 201 (UNS No 20100) as well as geometric properties such as lengths, aspect ratios and cross section geometries and dimensions- are assigned to calculate required components of element stiffness matrices. Stiffness matrices of all elements are assembled into a global stiffness matrix. Then loads are prescribed on the fiber networks by displacing the boundary by certain amount. Finally, established systems of equations are solved to obtain the nodal displacements. Nevertheless, these calculations are conducted by the internal solver of Strand7, which is commercially available finite element analysis software.

One of the important assumptions in the proposed finite element model is that contacts are completely rigid to avoid involvement of unnecessary nonlinearity due to contacts. For intricate models, like the ones in this study, computation costs would be enormously high which would obscure the benefits of employing non-linear solutions.

Fibers in the network are considered to be straight and have constant circular cross section with equal diameters. Fiber material is assumed to be made of a linearly elastic isotropic material which obeys Hooke's law. Fibers divided into smaller beam elements are modeled with Bernoulli and Timoshenko beams. Timoshenko beam model accounts for shear deformation, rotational inertia effects making this model

appropriate to low aspect ratio beams. However, Bernoulli beams do not take those parameters into account for simplicity. The discrepancy in the results obtained from two beam approaches will be investigated so that appropriate model will be employed in the rest of this study.

THEORETICAL METHOD

The geometries of fiber networks are created by the computer program according to the model discussed above. The created geometries are imported into the Strand7 for compression simulations and for calculation of Poisson's ratio and effective Young's modulus after stretching. Compressions are applied by displacing nodes in transverse direction into the networks. In order to standardize the compression a parameter, compression ratio c_r, is introduced. It is the ratio of the compressed height to the initial height of a compressed network and formulated in Eq.(2).

The initial height, l_y and the final height h. All compressions in the simulations are controlled by c_r for consistent deformations.

$$c_r = \frac{l_y - h}{l_y} \qquad (2)$$

Compressed fiber networks are saved as new networks for tensile simulations before the displacements are removed. However, curvatures of fibers are not conserved because Strand7 only saves the nodal locations. The saved networks are stretched in longitudinal direction for the calculation of Poisson's ratio and effective Young's modulus. At the end of the finite element analysis, solver returns the displacements and final locations of each node. In addition, the solver returns the nodal reaction forces on the boundaries. The nodal values of displacements and reaction forces so Eq.(3) can be employed to obtain Poisson's ratio, ν, and effective Young's modulus, E.

$$\nu = -\frac{\Delta t/t_0}{\Delta l/l_0} \quad E = \frac{\sum F_x/A_0}{\Delta l/l_0} \quad E' = \frac{E}{E_f} \qquad (3)$$

The average values of calculated Poisson's ratios and effective Young's moduli are both tabulated and graphed for different parameters to observe their effects. Standard deviations are also calculated and included in the graphs as well.

RESULTS

The fibers in the fiber mats are assumed to be linear elastic and obey Hooke's law. The fiber cross sections are considered to be circular whose diameters are constant throughout the fiber length. Fibers in the networks are modeled with Bernoulli beams since the initial aspect ratios of fibers are assumed to be larger than 10. Rigid connections are enforced on the points of intersections of fibers because fibers are assumed to be bonded at their intersections with each other.

Astrom et al. [27] included an angle at each intersection point of fibers in order to model the consequence of the compression conducted in the manufacturing of metal fibrous mats. A realistic model must incorporate any impacts resulted from the fabrication as well as the other considerations discussed in the previous section. The compression in the fabrication process causes change in fiber geometries while inducing stresses. However sintering at elevated temperatures releases the residual stresses induced from compression. The 2D fiber network discussed in this section incorporates the geometrical effects of compression by simulating the compression and preserving the final geometry created by compression while disregarding the initial stresses.

At the end of sintering process the fiber network, which is not undergone any compression, possesses the geometry of straight fibers shown in Fig.1. The fiber networks are compressed with a 75% amount as shown in Fig. 2. The fiber network is strained by 5% longitudinally and deforms into the geometry shown in Fig.3. The final deformed body illustrated in Fig.3 exhibits increase in the transverse direction as a result of longitudinal stretching. Similar to the experiments performed by Delannay [2] and simulations run by Astrom [27] negative Poisson's ratio arisen in random fiber networks.

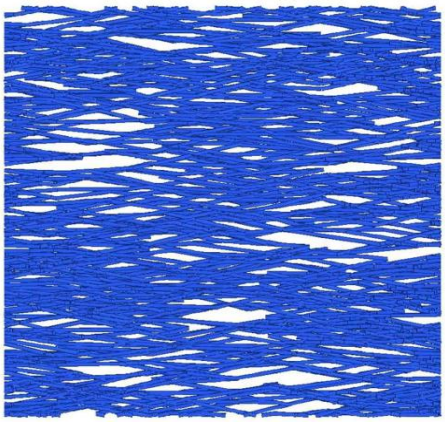

Figure 1: Uncompressed fiber network $\theta = \pm\pi/12$ fiber orientation

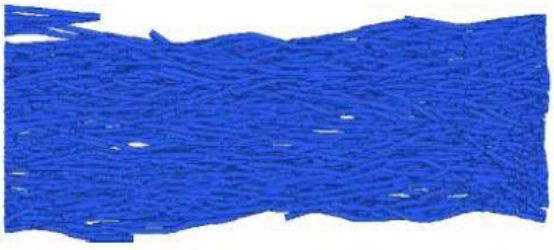

Figure 2: Fiber network compressed by 75% with $\theta = \pm\pi/12$ fiber orientation

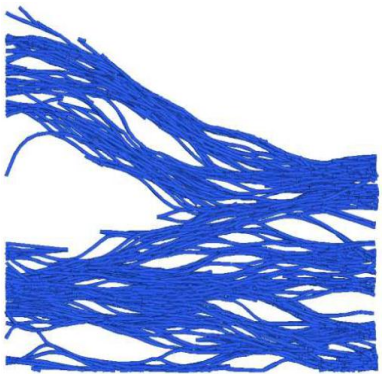

Figure 3: Fiber network compressed by 75% with $\theta = \pm\pi/12$ fiber orientation is stretched by 5%

COMPRESSION RATIO EFFECT

In this section, the effect of compression on Poisson's ratio and effective modulus will be investigated in detail. The compression can be imposed either by applying nodal loads or nodal displacements. However, with nodal forces, it is hard to enforce a specific compression ratio. Therefore, all compression is enforced with nodal displacements. The network generation code finds the upper nodes of the model at $y = 1$ and assigns finite displacements to the node on the $y = 1$ boundary. Similarly, nodes on the $y = 0$ and $x = 0$ boundaries are determined in the geometry development stage and symmetric boundary conditions are imposed. The nodes on the $x = 1$ boundary are set free. The upper nodes are displaced by specific values inducing required amounts of compression on the 2D fiber networks.

Then, this saved fiber network is imported back to the Strand7 for tension simulation. Similar to the compression case, network generation code imposes 5% stretching along the x-axis on nodes of the x=1 boundary. After stretching shown in Fig.3, the extraction in transverse direction of initially compressed network is observed yielding Poisson's ratio.

The substantial transformation of Poisson's ratio from a positive to a negative value is due to the compression added to the simulation process similar to the fabrication procedure. Therefore, compression is a decisive parameter on Poisson's ratio of 2D fiber networks. The compression is introduced in the simulation of fiber networks as described above. Similarly, Astrom et al. [27] developed an analytical model to determine the in-plane stiffness of compressed fiber mats in which compression of fibers were introduced with an angle. The amount of this angle was related to the amount of compression. The finite element analysis software is employed to simulate the compression more accurately.

Depending on fiber size and specific design considerations fiber networks are subjected to different amounts of compression. In this section, different compression ratios are imposed on identical 2D fiber networks in order to evaluate the effect of compression on Poisson's ratio and effective modulus. Compression of fiber networks can be done by two methods either, displacing the nodes or applying nodal forces. In this study fiber networks are compressed by displacing the nodes with some amount because the compression by nodal displacements yields more homogeneous deformation than compression by nodal loads. The parameters given in Table 1 are used to create identical 2D fiber networks in order to impose different compression ratios. The compression ratio is increased from 0% to 75%. For each data point, at least 15 simulations were run; Poisson's ratio and effective Young's modulus of 2D fiber networks are calculated according to the equation Eq.(3). The relation of compression ratio on Poisson's ratio is shown in Fig.4.

Table 1: Effect of compression ratio on Poisson's ratio of 2D fiber networks of $N = 900$, $L = 0.25$, $a = 25$, and $\theta = \pm\pi/12$

N	L	a	θ	c_r	ν	$dev(\nu)$
900	0.25	25	$\pm\pi/12$	0.000	13.65	0.8960
900	0.25	25	$\pm\pi/12$	0.250	9.07	1.5250
900	0.25	25	$\pm\pi/12$	0.375	2.63	2.0400
900	0.25	25	$\pm\pi/12$	0.500	-4.44	2.7680
900	0.25	25	$\pm\pi/12$	0.625	-15.19	3.5100
900	0.25	25	$\pm\pi/12$	0.750	-27.37	3.0600

Table 2: Effect of compression ratio on Poisson's ratio of 2D fiber networks of $N = 900$, $L = 0.25$, $a = 25$, and $\theta = \pm\pi/12$

N	L	a	θ	c_r	E'	$dev(E')$
900	0.25	25	$\pm\pi/12$	0.000	0.00556	0.000422
900	0.25	25	$\pm\pi/12$	0.250	0.00824	0.000728
900	0.25	25	$\pm\pi/12$	0.375	0.00933	0.000191
900	0.25	25	$\pm\pi/12$	0.500	0.01074	0.000716
900	0.25	25	$\pm\pi/12$	0.625	0.01309	0.001281
900	0.25	25	$\pm\pi/12$	0.750	0.01775	0.003233

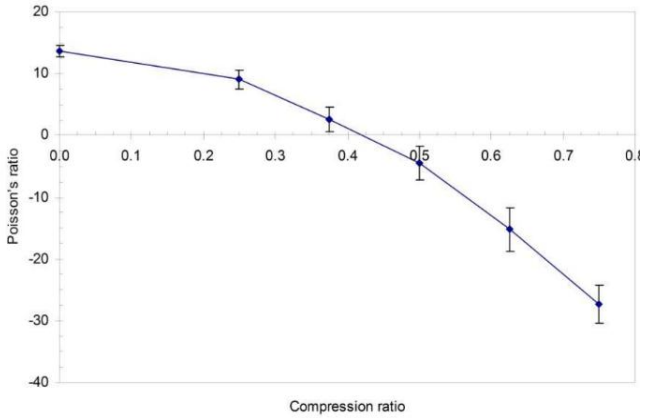

Figure 4: Effect of compression ratio on Poisson's ratio of 2D fiber networks of $N = 900$, $L = 0.25$, $a = 25$, and $\theta = \pm\pi/12$

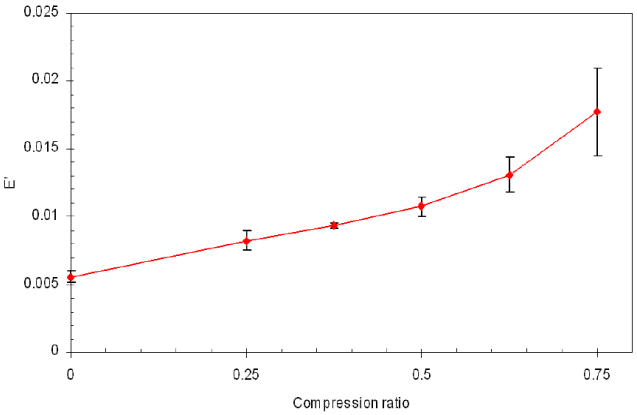

Figure 5: Effect of compression ratio on effective Young's modulus of 2D fiber networks of $N = 900$, $L = 0.25$, $a = 25$, and $\theta = \pm\pi/12$.

The compression ratio of the 2D fiber networks is increased gradually according to the data in Table 1. Poisson's ratio of the 2D fiber networks without any compression ratio is evaluated to be ν=13.65. However, as seen in Fig.4, ν approaches 0 between 37.5% and 50% compression. The Poisson's ratio becomes negative at 50% compression and further increases in the compression ratio increase the auxetic effect in fiber network.

Similarly, the relation of compression ratio on effective Young's modulus is calculated and given in Fig.5. Compression ratio is increased according from 0% compression to 75% compression gradually. The effective Young's modulus of 2D fiber networks is increases as the compression on the network increases as in Fig.5 according to data in Table 2. This is expected because as the compression increases the fiber density in a specific volume increases. Hence the number of load carrying fibers increases resulting higher E'.

EFFECT OF FIBER ORIENTATION

Anisotropy in fiber networks is related with the fiber orientation θ and the orientation distribution in the media. Since the fiber networks are not isotropic materials, the effect of anisotropy on mechanical properties are investigated in this section. Fibers can be deposited totally random or preferentially oriented in a specific direction to enhance the mechanical properties fiber networks. Fiber orientation can affect the auxetic properties of fiber mats.

The preliminary analyses presented that in-plane angle has also shown a significant effect on the deformation mechanism. Therefore, further simulations are performed to determine how the anisotropy, specifically in-plane angle θ governs the mechanical properties of E' and ν.

The fiber networks with different in-plane angles are developed to calculate the effect of anisotropy on Poisson's ratio and Young's modulus of 2D fiber networks. The restricted $\theta = \pm\pi/12$ in-plane angles brought to random orientation of in-plane angle $\theta = \pm\pi/2$ and results are drawn in Fig. 6. As it is

seen in Fig. 6 Poisson's ratio of fiber networks from a value of $\nu = -4.57$ to a value of $\nu = -0.066$ according to presented data in Table 2. These simulations show substantial dependence of Poisson's ratio on anisotropy or in-plane angle θ.

Effective Young's modulus E' of materials are also influenced by the anisotropy. Using the same simulations Young's moduli of fiber networks with different in-plane angles are calculated and tabulated in Table 3. The graph of effective Young's modulus with respect to in-plane angle is presented in Fig.7 in which a peek value exists around $\theta = \pm\pi/4$.

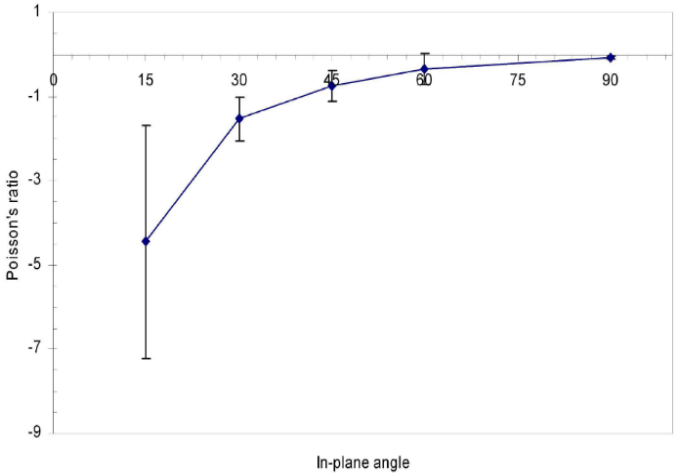

Figure 6: Effect of in-plane angle θ on Poisson's ratio of 2D fiber networks of $N = 900$, $L = 0.25$, $a = 25$, and $c_r = 0.5$.

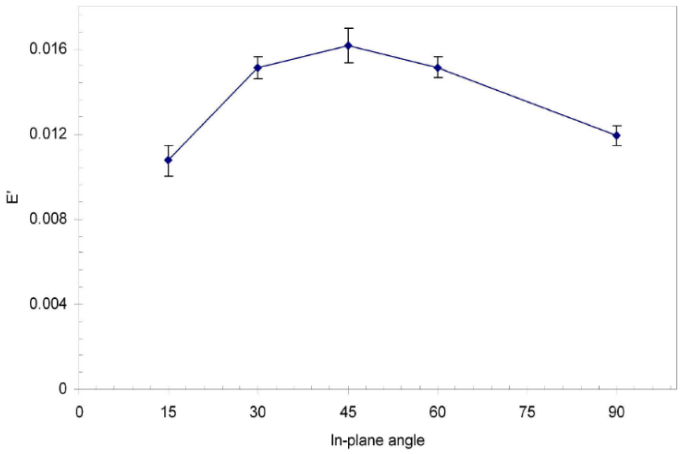

Figure 7: Effect of in-plane angle θ on effective oung's modulus of 2D fiber networks of $N = 900$, $L = 0.25$, $a = 25$, and $c_r = 0.5$.

Table 3: Effect of in-plane angle θ on Poisson's ratio of 2D fiber networks of $N = 900$, $L = 0.25$, $a = 25$, and $c_r = 0.5$.

N	L	a	θ	c_r	ν	$dev(\nu)$
900	0.25	25	$\pm\pi/12$	0.5	-4.44	2.7680
900	0.25	25	$\pm\pi/6$	0.5	-1.53	0.5308
900	0.25	25	$\pm\pi/4$	0.5	-0.74	0.3693
900	0.25	25	$\pm\pi/3$	0.5	-0.34	0.3601
900	0.25	25	$\pm\pi/2$	0.5	-0.07	0.0427

Table 4: Data for effect of in-plane angle θ on effective Young's modulus of 2D fiber networks.

N	L	a	θ	c_r	E'	$dev(E')$
900	0.25	25	$\pm\pi/12$	0.5	0.01074	0.000716
900	0.25	25	$\pm\pi/6$	0.5	0.01511	0.000528
900	0.25	25	$\pm\pi/4$	0.5	0.01615	0.000822
900	0.25	25	$\pm\pi/3$	0.5	0.01513	0.000485
900	0.25	25	$\pm\pi/2$	0.5	0.01193	0.000457

EFFECT OF ASPECT RATIO

Geometrical properties of each fiber as well as its mechanical properties affect the overall mechanical properties of fiber networks. Aspect ratios of fiber networks can be modified by changing either fiber length or diameter. In this section fiber lengths were kept constant while fiber diameters were modified in order to obtain specific aspect ratios. However, changes in fiber aspect ratios affect the number of fibers in the percolating cluster. The increase in aspect ratios develops different geometries by conserving more fibers in the percolating cluster and increases the number of contacts. Hence, same percolated fiber networks were utilized in each simulation. Therefore, the effect of aspect ratios on deformation is captured without any intervention of the other parameters.

The aspect ratio of the fiber network was increased gradually from a value of a=25 to a value $a = 200$ and tabulated in Table 4. The Poisson's ratio is calculated and presented in Fig.8. Despite the change in aspect ratio of fibers, Fig.8 does not exhibit a significant change in Poisson's ratio of 2D fiber networks. Poisson's ratios of the 2D fiber networks was evaluated around the value of $\nu \approx -12$. This result suggests that Poisson's ratio mostly depends on the geometry of the 2D fiber networks. If the compression is enforced by loads, the deflection of the fiber networks would be affected directly by the stiffness that depends on the aspect ratio of the beams. However, in this study compression is applied by displacing the upper nodes and specific displacement creates very similar geometrical fiber networks. Fiber networks are compressed to specific compressions regardless of fiber stiffness that depends on fiber aspect ratios.

Simulations, that are used to calculate the Poisson's ratio, are also utilized to calculate the effective Young's moduli of fiber networks with different aspect ratios. The results are given in the Table 5 and put in the Fig.9. Effective Young's moduli of fiber networks decrease as aspect ratios of fibers are increased in Fig.9. This is not unexpected because the stiffness of fibers composing the networks decreases with the increasing aspect ratio yielding a less overall stiffness in the fiber networks.

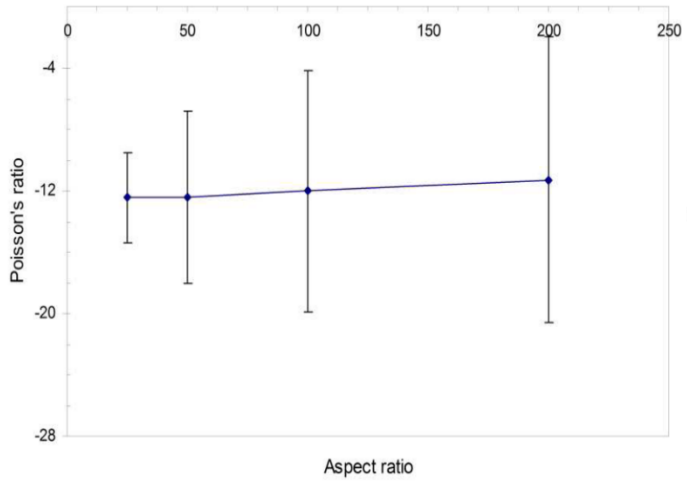

Figure 8: Effect of aspect ratio on Poisson's ratio of 2D fiber networks of $N = 900$, $L = 0.25$, $\theta = \pm\pi/12$, and $c_r = 0.5$.

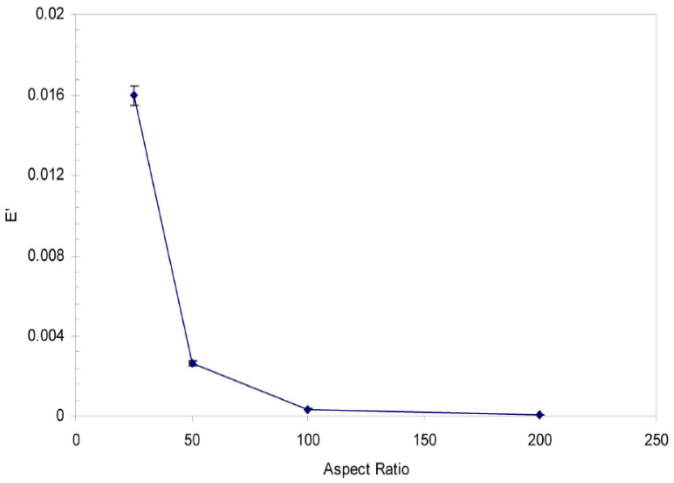

Figure 9: Effect of aspect ratio on effective Young's modulus of 2D fiber networks of N=900, L=0.25, θ=±π/12, and $c_r = 0.5$.

Table 5: Data for effect of aspect ratio on Poisson's ratio of 2D fiber networks.

N	L	a	θ	c_r	ν	$dev(\nu)$
900	0.25	25	$\pm\pi/12$	0.5	-12.46	2.93630
900	0.25	50	$\pm\pi/12$	0.5	-12.39	5.62306
900	0.25	100	$\pm\pi/12$	0.5	-12.02	7.88575
900	0.25	200	$\pm\pi/12$	0.5	-11.30	9.32916

Table 6: Data for effect of aspect ratio on effective Young's modulus of 2D fiber networks.

N	L	a	θ	c_r	E'	$dev(E')$
900	0.25	25	$\pm\pi/12$	0.5	0.015989879	0.000495463
900	0.25	50	$\pm\pi/12$	0.5	0.002624898	0.000133979
900	0.25	100	$\pm\pi/12$	0.5	0.000345055	4.30905E-05
900	0.25	200	$\pm\pi/12$	0.5	3.98883E-05	5.52811E-06

CONCLUSION

A comprehensive numerical model was developed to characterize the mechanical properties of 2D stainless steel fiber networks. The model employed in this study is intended to predict the effect of compression ratio, in-plane and out-of-plane angle variation, aspect ratio on effective Poisson's ratio and Young's modulus of fiber networks. Fundamental engineering principles of beam theories are utilized to model the fiber networks. Qualitative agreement between 2D and 3D models [28] illustrates the validity of these models.

One of the important conclusions of this study is the effect of the compression of fiber networks. Fiber networks that do not undergo any compressions do not show any auxetic behavior. Similar to degree of compression, fiber orientations in the network have a significant effect on the mechanical behavior of the network. Smaller in-plane angles in 2D networks yield better auxetic behavior.

This finite element model would provide a valuable development tool for the composite materials industry. Critical parameters can be identified, and their influence on the composite systems can be addressed without extensive experimentation. The properties of existing products can be improved. Innovative production technologies or new composites can be developed with the help of the model. Quantitative analysis will be performed for further comprehension of auxeticity in fiber networks.

REFERENCES

[1] G. Marsh. *Reinforced plastics*, 49 (3):26,32, 2005.

[2] F. Delannay. *International Journal of Solids and Structures*, 42:2264, 2005.

[3] M. Delince, F. Delannay. *Acta Materialia*, 52:1013, 2004.

[4] A. E. H. Love. A treatise on the mechanical theory of elasticity. Cambridge *A treatise on the mechanical theory of elasticity*. Cambridge University Press, Cambridge, 4th edition, 1927.

[5] D. J. Gunton, G. A. Saunders. *Journal of Materials Science*, 7:1061, 1972

[6] Y. Li. *Physica Status Solidi*, 38:171, 1976. [14] Y. Li. *Physica Status Solidi*, 38:171, 1976.

[7] R. H. Baughman, J. M. Schaklette, A. Zakhidov, Stafstorm. *Nature*, 392:362, 998

[8] N. R. Keskar, J. R. Chelikowsky. *Nature*, 358:222, 1992

[9] Y. Yeganeh-Haeri, D.J. Weidner, J.B. Parise. *Science*, 257:650, 1992.

[10] A. Alderson, K. L. Alderson, K. E. Evans, J. N. Grima, M. Williams. *Journal of Metastable and Nanocrystalline Materials*, 23:55, 2005.

[11] A. Alderson, K. E. Evans. *Physics and Chemistry of Minerals*, 28:711, 2001.

[12] A. Alderson, K. L. Alderson, K. E. Evans, J. N. Grima, M. R. Williams, P. J

[13] J. N. Grima, R. Gatt, A. Alderson, K. E. Evans. *Materials Science and Engineering A- Structural Materials Properties Microstructure and Processing*, 423:219, 2006

[14] J. N. Grima, R. Gatt, V. Zammit, J. J. Williams, K. E. Evans, A. Alderson, R.I. Walton. *Journal of Applied Physics*, 8:101, 2007.

[15] C. Lees, J. F. V. Vicent, J. E. Hillerton. *Biomedical Engineering*, page 19, 1991

[16] D. R. Veronda, R. A. Westmann. *Journal of Biomechanics*, 3:111, 1970.

[17] L. M. Frohlich, M. Labarbera, W. P. Stevens. *Journal of Zoology Lond.*, 232:231, 1994.

[18] J. L. Williams, J. L. Lewis. *Journal of Materials Science*, 23:4406, 1988.

[19] W. Yang, Z. Li, W. Shi, B. Xie, M. Yang. *Journal of Materials Science*, 23:4406, 1988.

[20] A. G. Steer, J. F. B. Payne. *International Atomic Energy Agency*, 104:50, 1982.

[21] I. A. Aksay, J. T. Groves, S. M. Gruner, P. C. Y. Lee, R. K. Prudhomme, W. Shih, S. Torquato, G. M. Whitesides. *SPIE International Society of Optical Engineers*, 2716:280, 1996.

[22] U. D. Larsen, O. Sigmund, S. Bouwstra. *Journal of Microelectromechanical*

[23] J. B. Choi, R. S. Lakes. *Journal of Materials Science*, 27:5375, 1992.

[24] R. S. Lakes. *World Patent No. 88/00523*, 1998.

[25] J. N. Grima, R. Gatt, N. Ravirala, A. Alderson, K. E. Evans. *Materials Science and Engineering A*, 423:214, 2006.

[26] B. D. Caddock, R. S. Lakes. *Journal of Physics D-Applied Physics*, 22:1877, 1989

[27] J. A. Astrom, J. P. Makinen, H. Hirvonen, J. Timonen. *Journal of Applied Physics*, 88:5066, 2000.

[28] Tatlıer, M., Berhan, L., Modelling the negative Poisson's ratio of compressed fused fiber networks, *Physica Status Solidi (b)*, 246 (9), 2018-2024, 2009